ZVS control strategy for four-switch buck-boost converter based on inductor peak current minimization method

Xueyang Ma*[a], Qifeng Xu[a,b], Yusheng Jiao[a]
[a]Application Satellite Power System Department, Shanghai Institute of Space Power-Sources, Shanghai 200245, China; [b]School of Aerospace Engineering, Xi'an Jiaotong University, Xi'an 710049, Shaanxi, China

ABSTRACT

This paper proposes a zero-voltage switching (ZVS) control strategy for a four-switch Buck-Boost (FSBB) converter that is easy to calculate and minimizes the peak value of the inductor current. Different from the complex calculation formula used in related studies to calculate the Root-Mean-Square (RMS) value of the inductor current, the proposed control method can equivalently achieve the control goal of minimizing the RMS value of the inductor current by calculating a simple expression for the peak value of the inductor current. At the same time, since no complex calculation is required, the computing power requirements for the microcontroller can be reduced, and the controller can complete real-time calculations at a higher frequency to achieve a more realistic and accurate control effect. In addition, the control strategy proposed in this paper only needs to store a small number of boundary limit curves. Since there is no need to store key calculation results, the requirements for the microcontroller FLASH space can be reduced. A 400 W FSBB converter simulation is performed to verify this method.

Keywords: Peak current minimization, four-switch buck-boost converter, ZVS

1. INTRODUCTION

As orbiting satellites enter and exit the Earth's shadow, environmental factors change dramatically, and the operating point of photovoltaic cells varies widely, which puts forward the demand for electric energy conversion with a wide voltage range for primary power supplies for aerospace. Wide input voltage range, high efficiency, and high-power density are the core indicators. For primary power supplies for aerospace, non-isolated DC/DC topology is often used. Figure 1 is a basic schematic diagram of the FSBB converter applied in a photovoltaic system. The four-switch Buck-Boost converter has the advantages of low voltage stress, step-up and step-down, high energy efficiency, small size, and wide input voltage range. At the same time, it can easily realize ZVS of the switches, reduce switching loss and noise, and improve electromagnetic compatibility performance. This converter is widely used in primary power products for aerospace and is an attractive research object.

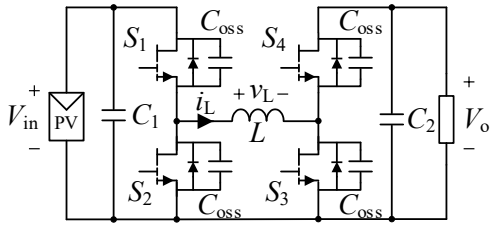

Figure 1. Four-switch buck-boost converter topology scheme used in PV system.

Figure 2 shows the driving waveform, inductor voltage waveform and inductor current waveform of the FSBB converter in the two working modes of DCM and CRM respectively under the quadrilateral inductor current modulation mode when the input voltage is greater than the output voltage. In many designs, the FSBB converter operates in the quadrilateral inductor current modulation (QCM) mode with buck-boost capability, and adopts the inductor current RMS value optimization strategy[1-4]. Under the quadrilateral inductor current modulation mode, the converter has two working

*mxy877532509@gmail.com

International Conference on Optics, Electronics, and Communication Engineering (OECE 2024), edited by Yang Yue, Proc. of SPIE Vol. 13395, 133950Q · © 2024 SPIE · 0277-786X · Published under a Creative Commons Attribution CC-BY 3.0 License · doi: 10.1117/12.3049137

waveforms, namely discontinuous conduction mode (DCM) and critical continuous mode (CRM). It works in CRM mode when fully loaded and in DCM mode when lightly loaded. The inductor current waveform of the converter is a quadrilateral with multiple degrees of freedom for optimization. The RMS value of the inductor current can be reduced through analytical algorithms to improve working efficiency.

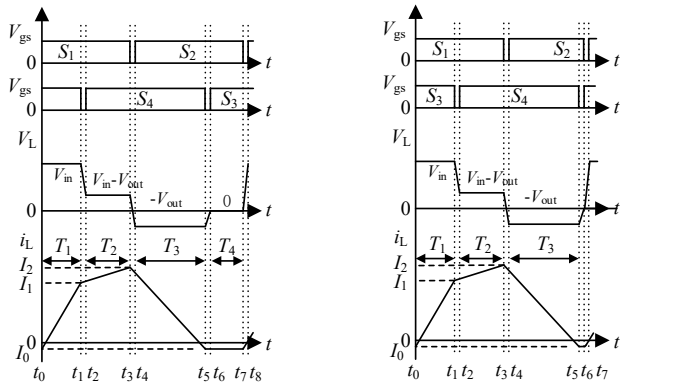

a) Discontinuous conduction mode(DCM) b) Critical continuous mode(CRM)

Figure 2. The driver waveform, inductor voltage and inductor current waveform of the converter in the DCM or CRM working modes respectively under quadrilateral inductor current modulation. (When $V_{in}>V_{out}$)

In recent years, there are three strategies for optimizing the RMS value of inductor current. This article summarizes these strategies as follows. The first control strategy[5-8] determines the conduction time of each switch by directly performing analytical solutions to the RMS value of the inductor current or the output power value, which can obtain direct and effective optimization effects and can adapt to different voltage, current and power ranges. However, due to the complexity of the expression, the microcontroller needs to use a look-up table and linear interpolation method to perform key operations, which requires the microcontroller to have a considerable amount of FLASH space. In addition, depending on the dimensionality of the look-up table, as well as the requirements for the input and output voltage range and output current range and the control accuracy requirements, the size of the look-up table may increase further, and the linear interpolation algorithm will become more complicated. This will impose a high computational burden on the microcontroller, and the consumed FLASH capacity will reach an unacceptable level. In general, this control strategy has high requirements on the storage space and computing power of the microcontroller.

The second control strategy is a strategy that aims to reduce the inductor current peak value in critical continuous mode[9]. This strategy is designed to be applied to the control method of variable frequency regulation in CRM mode, and does not extend the control method in DCM mode.

The third control strategy is a simplified real-time control strategy[10,11]. By setting the initial current value of the trapezoidal corner point (i.e., point t_1 in Figure 2) to the minimum current value that satisfies the ZVS condition, the PI controller is used to adjust the energy transfer time (i.e., time T_2 in Figure 2) to adjust the inductor current, thereby adjusting other variables. This algorithm is also a method of equivalently reducing the RMS value of the inductor current by reducing the inductor current peak value. This method is a simplified method that requires the PI controller to participate in the regulation of the inductor current peak value, which makes the PI parameter design not only highly coupled with the change of the inductor current peak value, but also deeply coupled with the change of the input and output voltages.

The control strategy given in this article is also a method of reducing the RMS value of the inductor current by reducing the peak value of the inductor current, thereby reducing the converter loss and improving the conversion efficiency. This article gives the analytical formula of the key switching time and the input, output voltage and output current, which has a certain degree of decoupling and is not too complicated. Since no complex calculations are required, the computing power requirements of the microcontroller can be reduced. Since there is no need to store key calculation results, the requirements for the microcontroller FLASH space can be reduced. This strategy can cover all operating conditions in DCM mode and equivalently minimize the RMS value of the inductor current.

2. PROPOSED ZVS CONTROL WITH MINIMIZED PEAK INDUCTOR CURRENT

2.1 Introduction of some basic variables and equations

This section summarizes the key current waveform expressions of the FSBB converter under QCM modulation, explicitly gives the relationship between circuit variables and multiple control variables, and finally gives equations to hold the ZVS condition. These expressions serve the derivation of the key equations in the next section.

Figure 3 shows the waveform of the inductor current when the input voltage is greater than, equal to, or less than the output voltage. I_0 represents the minimum value of the inductor current. After T_1, the inductor current reaches the first corner point I_1. After T_2, the inductor current reaches the second corner point I_2. After T_3, the inductor current drops to the minimum value I_0. The inductor current remains approximately unchanged during the T_4 period. During the t_0~t_1 phase, S_1 is turned on and S_2 is kept off; S_3 is kept on and S_4 is kept off. The inductor current rises rapidly in the positive direction, from a negative current to a positive current. The inductor charges and stores energy under the action of the input voltage V_{in}. Since S_4 is in the off state, no energy is transferred to the output side. During the t_1~t_2 phase, S_1 is kept on and S_2 is kept off; S_3 is kept off and S_4 is turned on. The positive inductor current continues to change with a smaller slope ($|V_{in}$-$V_o|/L$). While V_{in} charges and stores energy in the inductor, it also directly transfers energy to the output side. During the t_2~t_3 phase, S_1 is kept off and S_2 is turned on; S_3 is kept off and S_4 is kept on. The inductor current drops rapidly in the negative direction, from a positive current to a negative current, and the energy stored in the inductor is completely transferred to the output side. Since S_1 is in the off state, no energy is input to the converter. In the t_3~t_4 stage, S_1 is kept off and S_2 is kept on; S_3 is turned on and S_4 is kept off. The inductor current is negative and circulates in the loop S_2-S_3-L. The energy stored in the inductor will be consumed in the switches and the line impedance. The converter has no energy transmission to the outside. This mode exists in DCM mode and does not exist in CRM mode.

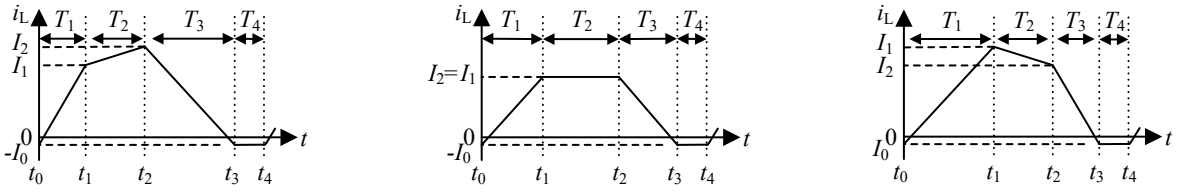

(a) $V_{in}>V_o$ (b) $V_{in}=V_o$ (c) $V_{in}<V_o$

Figure 3. Inductor current waveforms when input voltage is (a) greater than, (b) equal to, and (c) less than output voltage.

According to the basic volt-ampere relationship, the inductor current waveform expression corresponding to the current curve shown in Figure 3 can be obtained as shown in equation (1)[5].

$$i_L(t)=\begin{cases} -I_0+\dfrac{V_{in}}{L}t & 0\le t\le t_1 \\ -I_0+\dfrac{V_o}{L}t_1+\dfrac{V_{in}-V_o}{L}t & t_1\le t\le t_2 \\ -I_0+\dfrac{V_o}{L}t_1+\dfrac{V_{in}}{L}t_2-\dfrac{V_o}{L}t & t_2\le t\le t_3 \\ -I_0 & t_3\le t\le t_4 \end{cases} \tag{1}$$

where I_0 represents the minimum inductor current, V_{in} is the input voltage, and V_o is the output voltage. t_1-t_4 are the switching time points, which can be seen in Figure 3.

The parameter relationship within a cycle is as shown in equations (2)-(4)[8],

$$I_1+I_0=\frac{V_{in}}{L}T_1 \tag{2}$$

$$I_2-I_1=\frac{V_{in}-V_o}{L}T_2 \tag{3}$$

$$V_o\left(T_2+T_3\right)=V_{in}\left(T_1+T_2\right) \tag{4}$$

in which, I_0, I_1, and I_2 represent the current values of each corner point of the inductor current, and T_1, T_2, and T_3 represent the duration of each stage in which the slope of the inductor current remains unchanged.

The output power is provided by the inductor current of the T_2 and T_3 stages. By integrating this current, the output current I_{out} expression can be obtained as shown in equation (5).

$$I_{out}=\frac{1}{T_s}\left[\frac{T_2}{2}\left(I_1+I_2\right)+\frac{T_3}{2}\left(-I_0+I_2\right)\right] \tag{5}$$

where T_s represents the switching period.

Substituting equations (2)-(4) into equation (5), we can obtain the relationship between T_1 and T_2 in equation (6),

$$T_1=\frac{I_0L-T_2V_{in}+\sqrt{I_0^2L^2+2I_{out}T_sV_oL+V_{in}V_oT_2^2}}{V_{in}} \tag{6}$$

In order to determine the minimum negative and positive ZVS current values, according to the traditional design method, it is assumed that the inductor current remains unchanged during the four dead time instants of t_0, t_1, t_2, and t_3. Figure 4 shows the equivalent circuit of the ZVS process of the switches during the dead time. Considering the input and output voltages, the dead time t_d, and the equivalent output capacitance C_{oss} of the switches, a simple expression for the ZVS current value during each dead time can be given.

(a) Discharging process (b) Finish of the discharging process

Figure 4. Equivalent circuit example of the ZVS process at the dead time instant of t0.

The ZVS current value $I_{ZVS\_t0,t2}$ at t_0, t_2 is shown in equation (7).

$$I_{ZVS\_t0,t2}=\frac{V_{in}\cdot 2C_{oss}}{t_d} \tag{7}$$

The ZVS current value $I_{ZVS\_t1,t3}$ at t_1, t_3 is shown in equation (8).

$$I_{ZVS\_t1,t3}=\frac{V_{out}\cdot 2C_{oss}}{t_d} \tag{8}$$

2.2 Proposed ZVS control with minimum peak inductor current

Substituting the result of equation (6) into equation (1), we can get the expression of the peak current with respect to T_2 in equation (9), which represents the peak inductor current $I_{L,pk1}$ when $V_{in}>V_o$.

$$I_{L,pk1}=\frac{\sqrt{I_0^2L^2+2I_{out}T_sV_oL+V_{in}V_oT_2^2}}{L}-\frac{V_o}{L}T_2 \tag{9}$$

Equation (10) represents the peak inductor current $I_{L,pk2}$ when $V_{in}<V_o$.

$$I_{L,pk2}=\frac{\sqrt{I_0^2L^2+2I_{out}T_sV_oL+V_{in}V_oT_2^2}}{L}-\frac{V_{in}}{L}T_2 \tag{10}$$

The minimum inductor peak current is equivalent to the minimum RMS current, and the calculation of T_2 with the minimum peak current is simpler, so the current control with the minimum RMS value can be achieved according to this T_2. For equation (9), take the derivative of $I_{L,pk1}$ with respect to T_2 and set the derivative to zero, and the time T_2 when $I_{L,pk1}$ is minimum can be obtained as shown in equation (11).

$$T_2 = \sqrt{\frac{I_0^2 L^2 + 2 I_{out} T_s V_o L}{V_{in}^2 - V_{in} V_o}} \tag{11}$$

From equation (11), it can be seen that since the output voltage V_o, negative current I_0, inductance value L and switching period T_s are all constant values, T_2 increases as I_{out} increases, and as V_{in} approaches V_o, T_2 increases. In the process of V_{in} going from the maximum value to V_o, T_2 will rise to a large value, and then the sum of the calculated T_1, T_2, and T_3 times will exceed the switching period, making the control ineffective.

For equation (10), take the derivative of $I_{L,pk2}$ with respect to T_2 and set the derivative to zero, and the time T_2 when $I_{L,pk2}$ is the smallest can be obtained as shown in equation (12).

$$T_2 = \sqrt{\frac{I_0^2 L^2 + 2 I_{out} T_s V_o L}{V_o^2 - V_{in} V_o}} \tag{12}$$

It can be seen from equation (12) that T_2 also increases with the increase of I_{out}, and as V_{in} approaches V_o, T_2 increases. The characteristics shown in equation (12) are similar to those of equation (11). When V_{in} goes from the minimum value to V_o, T_2 will be too large and the control will fail.

The curve shown in Figure 5 can be drawn from equations (11) and (12), which shows the transformation curve of the normalized optimal T_2 time that can achieve the minimum RMS value of the inductor current under the input voltage V_{in} range and different output current conditions. The change trend of this value is the same as the above analysis.

For the optimal T_2 time mentioned above, its maximum value needs to be restricted. For simplicity, this paper implements this condition by limiting the sum of T_1, T_2, and T_3 time and the non-negative value of each time of T_1, T_2, and T_3. Solving the constraint condition expressed by equation (13), the T_2 time boundary range that ensures the effective implementation of the control strategy can be obtained, as shown in Figure 6a. For simplicity, the influence of PWM dead time t_d is ignored here.

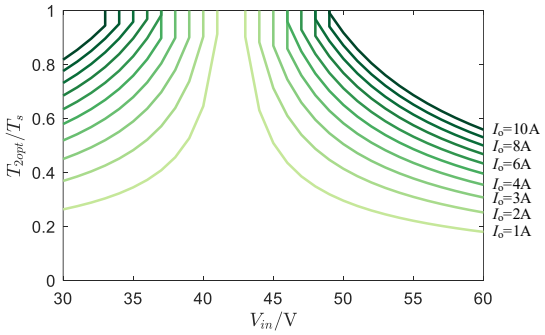

Figure 5. Normalized optimal T_2 time curve with respect to input voltage Vin (without considering boundary limits).

$$\begin{cases} T_1, T_2, T_3 > 0 \\ T_1 + T_2 + T_3 < T_s \end{cases} \tag{13}$$

By adding the restriction of Figure 6a to the curve shown in Figure 5, the restricted optimal T_2 time curve shown in Figure 6b can be obtained.

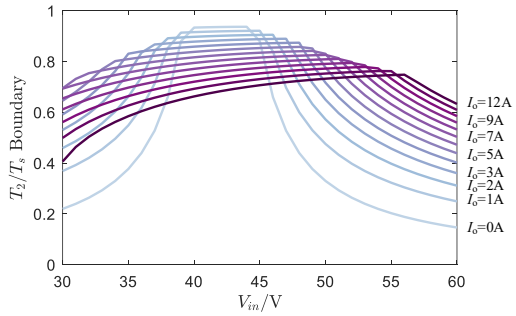

(a) T2 time boundary range curve to ensure effective implementation of control strategy under output voltage 42 V and different output currents

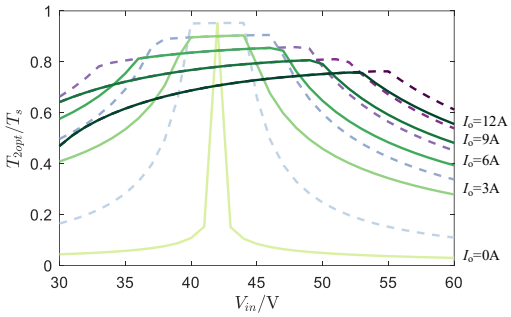

(b) The optimal time curve of T2opt (green solid line) and its boundary (purple dotted line) to ensure the effective implementation of the control strategy

Figure 6. T2 time boundary range curve to ensure effective implementation of the control strategy and the optimal T2 time curve after restriction.

The software closed-loop control process of the algorithm described in this paper is shown in Figure 7. In each control cycle, the microcontroller samples the output current I_{out}, input voltage V_{in}, output voltage V_o, and negative current I_0. After sampling, the output current is compared with the reference current signal, and the digital PI controller outputs the I_{outset} value. This value is used to perform the calculation of the decoupled calculation formula, that is, according to the relationship between the input and output voltages, equation (11) or (12) is selected for calculation to obtain the optimal T_2 value. Then, the optimal T_2 value is limited by a small amount of pre-stored limit data. After that, the T_1 value is calculated by a fixed functional relationship. Then T_1, T_2 and I_0 determine the output PWM waveform. The role of I_0 is to limit the negative current to a preset value to ensure the ZVS condition.

It is worth noting that T_1 can be solved directly through T_2, but the reverse is extremely difficult. The advantage of the proposed algorithm in this paper is that the expression of T_2 is concise and each control variable is easy to derive in sequence. It does not generate much calculation and does not require much FLASH space, and has a decoupling effect.

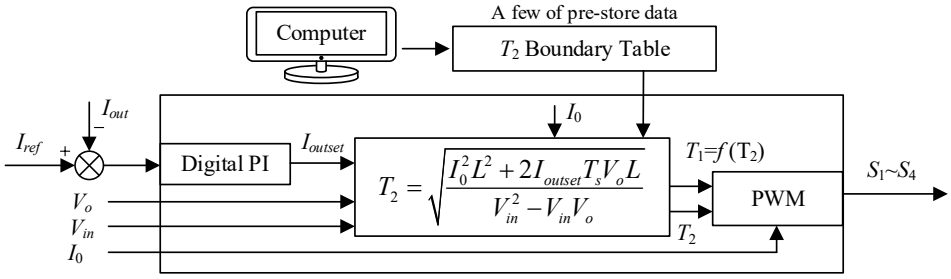

Figure 7. Closed-loop control diagram of the proposed minimum peak inductor current control strategy.

3. EXPERIMENTAL VERIFICATIONS

This paper follows the control strategy and process described in the previous chapter, designs a 400 W FSBB converter hardware with an input voltage range of 30-60 V, an output voltage range of 38-42 V, a maximum output current of 10 A, an inductance of 660 nH, and a switching frequency of 500 kHz. The switches used are GS61008P, of which the C_{oss} capacitance is 250 pF and the $R_{ds(on)}$ resistance is 7 mΩ. Figure 8 is the simulation schematic. The control method described in this paper has been verified on this simulation platform.

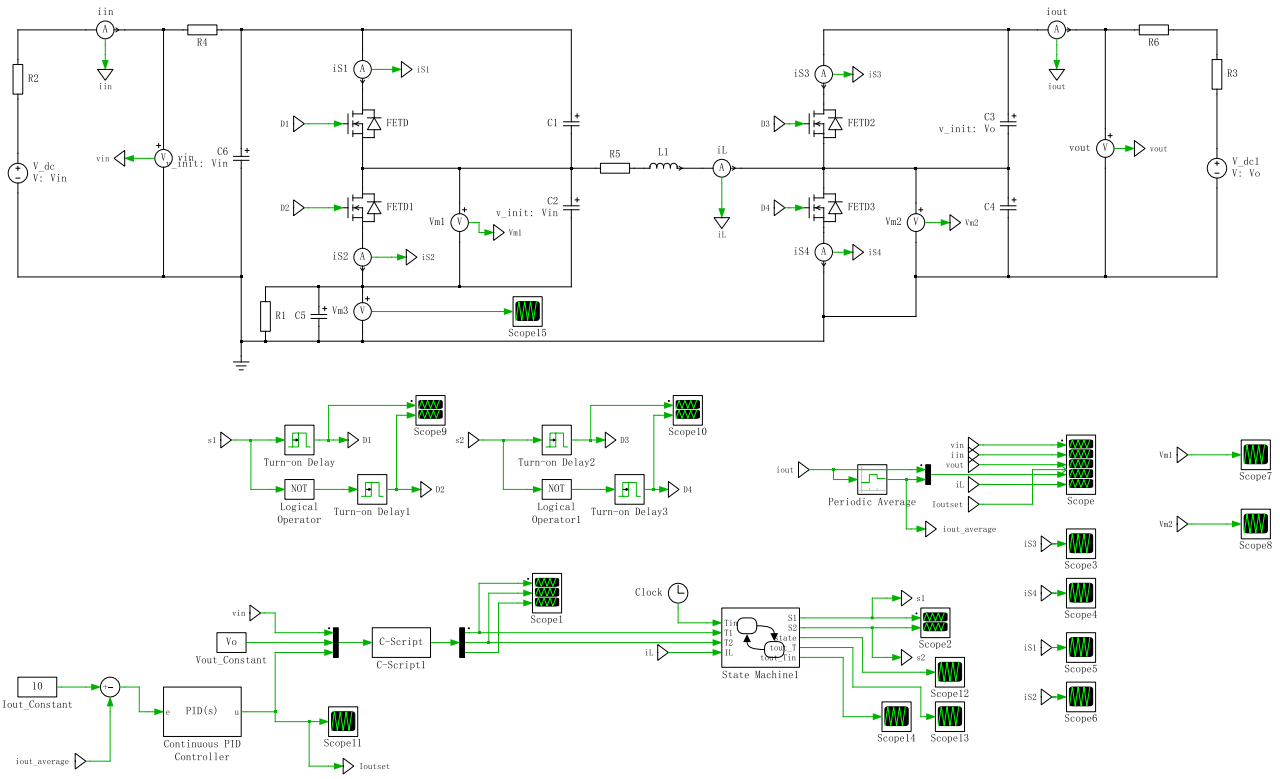

Figure 8. The FSBB hardware simulation scheme.

As shown in Figure 9, the amplitudes of the negative and positive currents are consistent with the design values, achieving zero-voltage turn-on of the switches, which can greatly reduce switching losses, increase the operating frequency, and achieve miniaturization and lightweight of the converter.

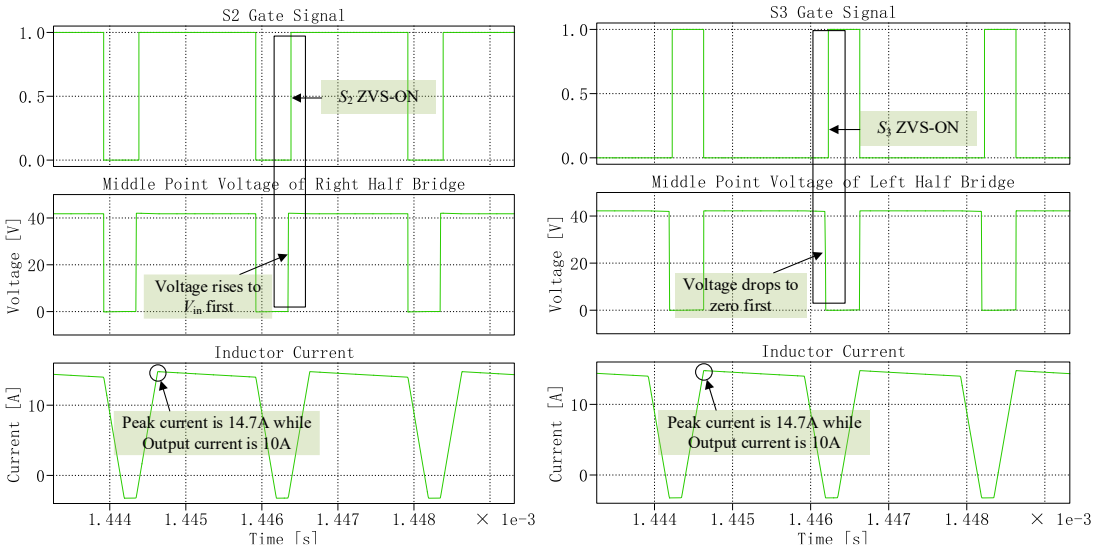

Figure 9. The ZVS waveform of S_2 and S_3(@ I_o=10 A) and closed-loop current control verification.

In terms of efficiency, at the 42~42 V operating point, the peak efficiency is 99.5% and the power is about 400 W. In addition, when the output voltage is close to the input voltage, such as 42~42 V, the proposed control method makes the volt-second value in the inductor very small, and the T_2 interval is the main interval, which is directly conducted from the

input to the output, achieving high efficiency. When the input voltage rises to 30 or 60 V, the RMS value and peak value of the inductor current are lower than the traditional buck-boost control, and the peak efficiency remains at 98.5%. This simulation experiment achieves the purpose of verifying the control scheme and proves that the control strategy is feasible.

4. CONCLUSION

In this paper, a ZVS control strategy for minimizing the inductor peak current is proposed. The strategy reduces the RMS value of the inductor current of the FSBB converter under ZVS control by mathematical decoupling. In the proposed control method, the calculation is successfully simplified by equivalent the RMS value calculation to the peak value calculation. In addition, the proposed method also greatly reduces the FLASH usage of the MCU. Therefore, the application of this strategy in high-frequency real-time computing systems will bring more practicality and convenience to mainstream MCUs, and enable the FSBB topology to have better power density and higher application efficiency. Verified by the FSBB simulation circuit, the peak conversion efficiency can reach over 98.5%.

REFERENCES

[1] Bai, Y., Cao, Y., Mitrovic, V., Fan, B., Burgos, R. and Boroyevich, D., "A simplified quadrangle current modulation for four-switched buck-boost converter (FSBB) with a novel small signal model," IEEE Appl. Power Electron. Conf. Expo., 736-743 (2023).

[2] Waffler, S. and Kolar, J. W., "A novel low-loss modulation strategy for high-power bidirectional buck + boost converters," IEEE Trans. Power Electron., 24(6), 1589-1599 (2009).

[3] Liu, Q., Qian, Q., Ren, B., Xu, S., Sun, W. and Li, H., "A new modulation strategy for four-switch buck-boost converter with reduced freewheeling current," IEEE Appl. Power Electron. Conf. Expo., 2104-2108 (2020).

[4] Liu, Q., Zheng, D., Zheng, M., Qian, Q., Xu, S. and Sun, W., "A high-power-density four-switch buck-boost converter using 3D multi-PCB structure," IEEE Appl. Power Electron. Conf. Expo., 16-19 (2021).

[5] Waffler, S., [Hochkompakter Bidirektionaler DC-DC-Wandler für Hybridfahrzeuge], Zurich: Diss Dgenssische Technische Hochschule Eth Zürich Nr, Doctor's Thesis, (2013).

[6] Waffler, S. and Kolar, J. W., "A Novel low-loss modulation strategy for high-power bidirectional buck+boost converters," IEEE Trans. Power Electron. 24, 1589-1599 (2009).

[7] Liu, Q., Qian, Q., Zheng, M., Xu, S., Sun, W. and Wang, T., "An improved quadrangle control method for four-switch buck-boost converter with reduced loss and decoupling strategy," IEEE Trans. Power Electron. 36, 10827-10841 (2021).

[8] Zhou, Z., Li, H. and Wu, X., "A constant frequency ZVS control system for the four-switch buck-boost DC-DC converter with reduced inductor current," IEEE Trans. Power Electron. 34, 5996-6003 (2019).

[9] Xia, K., Li, Z., Qin, Y., Yuan, Y. and Yuan, Q., "Minimising peak current in boundary conduction mode for the four-switch buck-boost DC/DC converter with soft switching," IET Power Electronics 12, 944-954 (2019).

[10] Tian, L., Wu, X., Zhou, Z. and Muhammad, F., "The MPPT application of the FSBB converter with MHz ZVS digital control," 2022 IEEE International Power Electronics and Application Conference and Exposition (PEAC) 1409-1413 (2022).

[11] Tian, L., Wu, X., Jiang, C. and Yang, J., "A simplified real-time digital control scheme for ZVS four-switch buck-boost with low inductor current," IEEE Trans. Ind. Electron. 69, 7920-7929 (2022).